J Therm Anal Calorim (2011) 103:131–135
DOI 10.1007/s10973-010-1082-4

Thermodynamic optimization of the Yb–Sn system

Mohamed Idbenali · Colette Servant

Received: 2 July 2010 / Accepted: 30 September 2010 / Published online: 21 October 2010

Abstract The thermodynamic optimization of the Yb–Sn binary system was carried out with the help of the CALPHAD (CALculation of PHAse Diagram) method. Yb_2Sn, α-βYb_5Sn_3, Yb_5Sn_4, YbSn, Yb_3Sn_5, and $YbSn_3$ have been treated as stoichiometric compounds, while a sublattice model has been used for the description of the liquid, BCC, BCT, and FCC phases. The calculations based on the thermodynamic modeling are in good agreement with the phase diagram data and experimental thermodynamic values.

Keywords Yb–Sn system · Phase diagram · Thermodynamic optimization · Calphad method

Introduction

This study is a part of a thermodynamic investigation of the R–Sn systems (R=La) [1] which is intended to give a better understanding of the constitutional properties and potential technological applications of these alloys.

This study deals with an assessment of the thermodynamic description of the Yb–Sn system using the CALPHAD technique [2]. The thermodynamic parameters involved in the models are optimized from the experimental thermodynamic and phase diagram data.

Review of experimental data

The assessed Yb–Sn phase diagram by Palenzona and Cirafici [3] is based on the work of Palenzona and Cirafici [4]. According to this assessment, five intermetallic compounds were reported ($YbSn_3$, YbSn, Yb_5Sn_4, Yb_5Sn_3, and Yb_2Sn). For the $YbSn_3$ and Yb_2Sn compounds, a congruent melting was determined, respectively, at 1078 and 1658 K, while for the YbSn, Yb_5Sn_4, and Yb_5Sn_4 (α and β) compounds, a peritectic formation was reported, respectively, at 1308, 1433, and 1508 K. A polymorphic transition ($\alpha \leftrightarrow \beta$) was determined at 1363 K for Yb_5Sn_4. In addition, two more phases were reported in recent papers, namely Yb_3Sn_5 [5] (see Fig. 1) and $Yb_{36}Sn_{23}$ [6]. The investigation of the Yb–Sn phase diagram is severely hampered by the high oxidability of the alloys in the central part of the system [3]. Moreover, a careful investigation on two of the phases reported in the assessment, namely Yb_3Sn_5 and Yb_5Sn_4, has shown that in the Yb–Sn system, these phases are stabilized by hydrogen impurity [7]. The crystal structures of the various phases of the Yb–Sn system are reported in Table 1.

Many authors [8–10] determined the enthalpies of formation for the intermetallic compounds of the Yb–Sn system; Palenzona [8] measured the standard enthalpy of formation of $YbSn_3$ using the dynamic differential calorimetry method. Colinet et al. [9] calculated by a semi-empirical model the enthalpies of formation of $YbSn_3$ [10] determined the enthalpies of formation for two intermetallic compounds Yb_5Sn_4 and Yb_5Sn_3.

It was presented at JEEP2010 Montpellier, France

M. Idbenali (✉)
Laboratoire de Thermodynamique Métallurgique et Rhéologie des Matériaux, Université Ibn Zohr, Dcheira, B.P. 496 Agadir, Morocco
e-mail: idbenalimohamed@yahoo.fr

C. Servant
Laboratoire de Physicochimie de l'Etat Solide, ICMMO, Université de Paris-Sud, 91405 Orsay Cedex, France

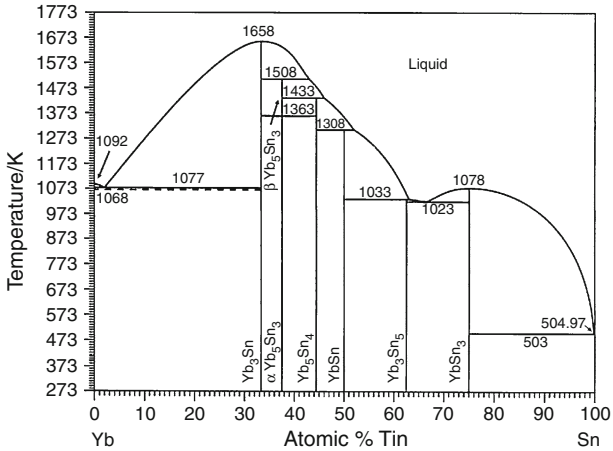

Fig. 1 The Yb–Sn system. Phase diagram revised in the composition range between 55 and 70 at.%Sn by Manfrinetti et al. [5]

Thermodynamic models

Pure elements

The Gibbs energy function

$$G_i^{\phi}(T) = {}^0G_i^{\phi} - H_i^{\mathrm{SER}}(298.15) \tag{1}$$

(298.15 K) for the element i (i = Yb, Sn) in the phase Φ (Φ = Liquid, BCC_A2, HCP_A3, BCT_A5, or FCC_A1) is described by an equation of the following form:

$$G_i^{\phi}(T) = a + bT + cT\ln T + \mathrm{d}T^{-2} + eT^3 + fT^7 + gT^{-9}, \tag{2}$$

where H_i^{SER} (298.15 K) is the molar enthalpy of the element i at 298.15 K in its standard element reference (SER) state, FCC_A1 for Yb and BCT_A5 for Sn.

In this article, the Gibbs energy functions are taken from the SGTE compilation of Dinsdale [11].

Solution phases

The solution phases [(γYb), β(Yb), α(Yb), β(Sn), and liquid] were modeled as substitutional solutions according to the polynomial Redlich–Kister model [12]. The Gibbs energy of 1 mol of formula unit of phase ϕ is expressed as the sum of the reference part ${}^{\mathrm{ref}}G^{\phi}$, the ideal part ${}^{\mathrm{id}}G^{\phi}$, and the excess part ${}^{\mathrm{xs}}G^{\phi}$:

$$G_m^{\phi} = {}^{\mathrm{ref}}G^{\phi} + {}^{\mathrm{id}}G^{\phi} + {}^{\mathrm{xs}}G^{\phi}. \tag{3}$$

As used in the Thermo-Calc software [13]:

$${}^{\mathrm{ref}}G^{\phi}(T) = \left({}^0G_{\mathrm{Yb}}^{\phi}(T) - H_{\mathrm{Yb}}^{\mathrm{SER}}(298.15)\right)x_{\mathrm{Yb}} + \left({}^0G_{\mathrm{Sn}}^{\phi}(T) - H_{\mathrm{Sn}}^{\mathrm{SER}}(298.15)\right)x_{\mathrm{Sn}} \tag{4}$$

$${}^{\mathrm{id}}G^{\phi} = RT(x_{\mathrm{Sn}}\ln x_{\mathrm{Sn}} + x_{\mathrm{Yb}}\ln x_{\mathrm{Yb}}) \tag{5}$$

where R is the gas constant, T the temperature, in Kelvin, x_{Sn} and x_{Yb} are the mole fraction of elements Sn and Yb, respectively.

The excess terms of all the phases were modeled by the Redlich–Kister [12] formula.

$${}^{\mathrm{xs}}G_m^{\phi}(T) = x_{\mathrm{Sn}}x_{\mathrm{Yb}}\left({}^0L_{\mathrm{Sn,Yb}}^{\phi}(T) + {}^1L_{\mathrm{Sn,Yb}}^{\phi}(T)(x_{\mathrm{Sn}} - x_{\mathrm{Yb}}) + {}^2L_{\mathrm{Sn,Yb}}^{\phi}(T)(x_{\mathrm{Sn}} - x_{\mathrm{Yb}})^2 + \cdots\right) \tag{6}$$

with

$${}^iL_{\mathrm{Sn,Yb}}^{\phi}(T) = a_i + b_iT \tag{7}$$

Table 1 Symbols and crystal structures of the stable solid phases in the (Yb–Sn) alloys from [3, 5]

Diagram symbol	Composition/ at.%Yb	Symbol used in Thermo-Calc data file	Pearson symbol	Space group	Struktur-bericht designation	Prototype
βSn	0	BCT	*tI4*	$I4_1/amd$	*A5*	βSn
αSn	0	Diamond	*cF8*	$Fd\bar{3}m$	*A5*	C (diamond)
YbSn3	25	YbSn3	*cP4*	$Fm\bar{3}m$	$L1_2$	$AuCu_3$
YbSn	50	YbSn	*tP2*	*P4/mmm*	$L1_0$	AuCu-I
Yb_5Sn_4	55.6	Yb_5Sn_4	*oP36*	*Pnma*	–	Gd_5Si_4
βYb_5Sn_3	62.5	Yb_5Sn_3-HT	*tI32*	*I4/mcm*	$D8_l$	Cr_5B_3
αYb_5Sn_3	62.5	αYb_5Sn_3-LT	*hP16*	$P6_3/mcm$	$D8_8$	Mn_5Si_3
Yb_2Sn	66.7	Yb_2Sn	*hP6*	$P6_3/mcm$	$B8_2$	Ni_2In
γYb	100	BCC	*cI2*	$Im\bar{3}m$	*A2*	W
βYb	100	FCC	*cF4*	$Fm\bar{3}m$	*A1*	Cu
αYb	100	HCP	*hP2*	$P6_3/mmc$	*A3*	Mg

where ${}^{i}L^{\phi}_{\mathrm{Sn,Yb}}(T)$ is the ith interaction parameter between the elements Sn and Yb, which is evaluated in the presented work, a_i and b_i are the coefficients to be optimized.

Stoichiometric compounds

The Gibbs energy of the stoichiometric compound ${}^{0}G_{\mathrm{ApBq}}$ is expressed as follows:

$$ {}^{0}G_{\mathrm{ApBq}} = \frac{p}{p+q}{}^{0}G_A + \frac{q}{p+q}{}^{0}G_B + a + bT, \quad (8) $$

where ${}^{0}G_A$ and ${}^{0}G_B$ are the Gibbs energy of the pure elements Sn and Yb, respectively, a and b are parameters to be determined.

Results and discussions

The evaluation of the thermodynamic parameters has been carried out using the PARROT [14] module in the Thermo-Calc code [13], takes various types of experimental data for the optimisation process. Data for the pure elements have been taken from the SGTE compilation [11]. Most of the experimental data are mentioned in "Review of experimental data" section. In the present parameter optimization procedure, we first imposed the conditions $d^2G/dx^2 > 0$ for modeling the liquid phase using the phase boundary data reported by [5] and thermodynamic data. We then modeled the parameters of the intermetallic phases beginning with the congruent melting (Liq $\Leftrightarrow$ Yb_2Sn). Finally, all the parameters of the different phases were simultaneously optimized with the experimental data mentioned above by imposing additional constraints to avoid the appearance of unwanted inverted miscibility gap in the liquid phase during the phase diagram calculation as recommended in [15–17]. All the parameters were evaluated and listed in Table 2.

The calculated phase diagram is shown in Fig. 2. The experimental and calculated temperatures of the invariant reactions are compared in Table 3. They are in very good agreement. The measured and calculated enthalpies of formation of the intermetallic compounds are presented in Fig. 3. They are in reasonable agreement.

The optimized temperature of the polymorphic transition (1090 °C) of $\alpha Yb_5Sn_3 \Leftrightarrow \beta Yb_5Sn_3$ chosen in [4] is in agreement with the calculated one (1087 °C). The enthalpies of formation of the two polytypes, αYb_5Sn_3 and $\alpha Yb_5Sn_3 \Leftrightarrow \beta Yb_5Sn_3$, are very similar and confirm the conclusion by Stein et al. [18] concerning the small structural energies of the different Laves phases polytypes. As mentioned in [17], in order to check that the optimized thermodynamic parameters of the intermetallic compounds are satisfactory, we verified that when the

Table 2 The optimised thermodynamic parameters of the Yb–Sn system

Phase	Thermodynamic models	Parameters in SI
Liquid	$(Yb, Sn)_1$	${}^{0}L^{\mathrm{Liq}}_{\mathrm{Yb,Sn}} = -155596.489 - 1.4010837T$
		${}^{1}L^{\mathrm{Liq}}_{\mathrm{Yb,Sn}} = -3736.52101$
		${}^{2}L^{\mathrm{Liq}}_{\mathrm{Yb,Sn}} = 36185.9184$
BCC_A2	$(Yb, Sn)_1(Va)_3$	No excess term
FCC_A1	$(Yb, Sn)_1 (Va)_1$	No excess term
YbSn3	$(Yb)_{0.25}:(Sn)_{0.75}$	$G^{\mathrm{YbSn_3}}_{\mathrm{Yb:Sn}} - 0.25\,{}^{298}H^{\mathrm{FCC\_A1}}_{\mathrm{Yb}} - 0.75\,{}^{298}H^{\mathrm{BCT\_A5}}_{\mathrm{Sn}} = 0.25\,{}^{298}G^{\mathrm{FCC\_A1}}_{\mathrm{Yb}} + 0.75\,{}^{298}G^{\mathrm{BCT\_A5}}_{\mathrm{Sn}} - 41797.2855 + 2.550250 52T$
YbSn	$(Yb)_{0.5}:(Sn)_{0.5}$	$G^{\mathrm{YbSn}}_{\mathrm{Yb:Sn}} - 0.5\,{}^{298}H^{\mathrm{FCC\_A1}}_{\mathrm{Yb}} - 0.5\,{}^{298}H^{\mathrm{BCT\_A5}}_{\mathrm{Sn}} = 0.5\,{}^{298}G^{\mathrm{FCC\_A1}}_{\mathrm{Yb}} + 0.5\,{}^{298}G^{\mathrm{BCT\_A5}}_{\mathrm{Sn}} - 55077.4602 + 0.646652440T$
Yb_5Sn_4	$(Yb)_{0.556}:(Sn)_{0.444}$	$G^{\mathrm{Yb5Sn_4}}_{\mathrm{Yb:Sn}} - 0.556\,{}^{298}H^{\mathrm{FCC\_A1}}_{\mathrm{Yb}} - 0.444\,{}^{298}H^{\mathrm{BCT\_A5}}_{\mathrm{Sn}} = 0.556\,{}^{298}G^{\mathrm{FCC\_A1}}_{\mathrm{Yb}} + 0.444\,{}^{298}G^{\mathrm{BCT\_A5}}_{\mathrm{Sn}} - 56787.7363 + 1.376727 39T$
βYb_5Sn_3	$(Yb)_{0.625}:(Sn)_{0.375}$	$G^{\beta\mathrm{Yb_5Sn_3}}_{\mathrm{Yb:Sn}} - 0.625\,{}^{298}H^{\mathrm{FCC\_A1}}_{\mathrm{Yb}} - 0.375\,{}^{298}H^{\mathrm{BCT\_A5}}_{\mathrm{Sn}} = 0.625\,{}^{298}G^{\mathrm{FCC\_A1}}_{\mathrm{Yb}} + 0.375\,{}^{298}G^{\mathrm{BCT\_A5}}_{\mathrm{Sn}} - 57602.0929 + 0.337700156T$
αYb_5Sn_3	$(Yb)_{0.625}:(Sn)_{0.375}$	$G^{\alpha\mathrm{Yb_5Sn_3}}_{\mathrm{Yb:Sn}} - 0.625\,{}^{298}H^{\mathrm{FCC\_A1}}_{\mathrm{Yb}} - 0.375\,{}^{298}H^{\mathrm{BCT\_A5}}_{\mathrm{Sn}} = 0.625\,{}^{298}G^{\mathrm{FCC\_A1}}_{\mathrm{Yb}} + 0.375\,{}^{298}G^{\mathrm{BCT\_A5}}_{\mathrm{Sn}} - 58406.1714 + 3.215336 68T$
Yb_2Sn	$(Yb)_{0.667}:(Sn)_{0.333}$	$G^{\mathrm{Yb_2Sn}}_{\mathrm{Yb:Sn}} - 0.667\,{}^{298}H^{\mathrm{FCC\_A1}}_{\mathrm{Yb}} - 0.333\,{}^{298}H^{\mathrm{BCT\_A5}}_{\mathrm{Sn}} = 0.667\,{}^{298}G^{\mathrm{FCC\_A1}}_{\mathrm{Yb}} + 0.333\,{}^{298}G^{\mathrm{BCT\_A5}}_{\mathrm{Sn}} - 57560.2159 + 3.508466 94T$

(Va) for vacancy

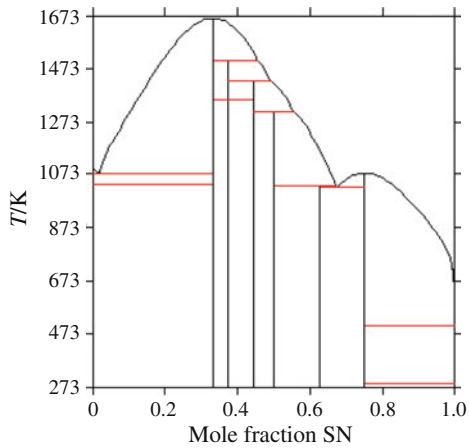

Fig. 2 Calculated Yb–Sn phase diagram

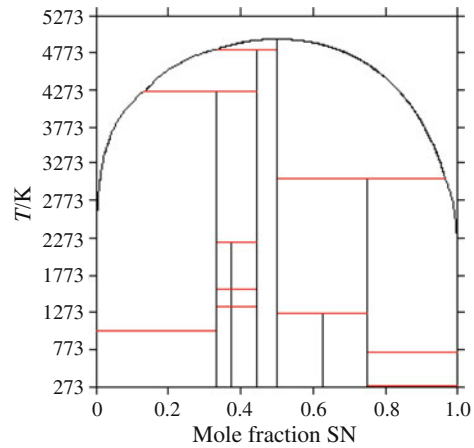

Fig. 4 Calculated La–Pb phase diagram when the liquid phase is suspended

Table 3 Invariant reactions in the Yb–Sn system

Reaction	Refs. [3, 5]		This work	
	T/K	x_{Liq}/at.%Yb	T/K	x_{Liq}/at.%Yb
Liq ⇔ βSn + $YbSn_3$	503	0.005	505	0.000045
Liq ⇔ $YbSn_3$	1078		1076	
Liq ⇔ $YbSn_3$ + Yb_3Sn_5	1023	0.33	1026	0.324
Liq ⇔ Yb_3Sn_5 + YbSn	1033	0.375	1032	0.33
Liq + Yb_5Sn_4 ⇔ YbSn	1308	0.48	1311	0.44
Liq + βYb_5Sn_3 ⇔ Yb_5Sn_4	1433	0.53	1428	0.507
Liq + Yb_2Sn ⇔ βYb_5Sn_3	1508	0.57	1505	0.543
αYb_5Sn_3 ⇔ βYb_5Sn_3	1363	–	1360	
Liq ⇔ Yb_2Sn	1658	0.667	1663	0.667
Liq ⇔ Yb_2Sn + γYb	1077	0.98	1074	0.98

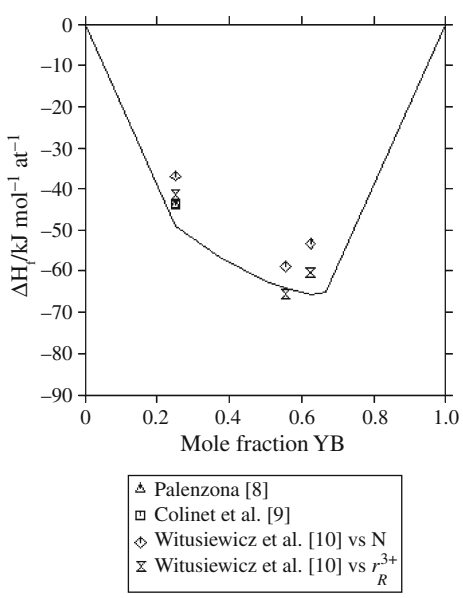

Fig. 3 Calculated and measured enthalpies of formation of the intermetallic compounds

liquid phase is suspended during the calculation of the Yb–Sn phase diagram, the stoichiometric phases disappear at high temperatures, the terminal solid solutions and a two-phase domain existing between them are calculated, Fig. 4. In the present case, the entropies of the intermetallic compounds are either negative (s = −b optimized positive value; Table 2) and lower than 3.5 J/mol K. It will be noted that only the (Yb–Sn) BCC_A2 solid solution is calculated on the whole Yb composition range and not the BCT_A5 (βSn) one in the Sn-rich region. This is due to the power series in terms of temperature for the Sn element in the BCC_A2 state which becomes metastable compared with the BCT_A5 state at higher temperatures [11].

Conclusions

A consistent set of thermodynamic parameters of the different phases of the Yb–Sn binary system has been optimized.

The computed values are in good agreement with the experimental data. We verified that no unwanted inverted miscibility gap was calculated for the solution phases.

Further thermodynamic determinations in particular for the liquid phase will be necessary to improve the assessment.

References

1. Idbenali M, Servant C, Selhaoui N, Bouirden L. A thermodynamic reassessment of the La_Sn system. Calphad. 2009;33:398–404.
2. Kaufman L, Bernstein H. Computer calculations of phase diagrams. New York, NY: Academic Press; 1970.
3. Palenzona A, Cirafici S. The Sn–Yb (Tin–Ytterbium) system. J Phase Equilib. 1991;12:482–5.

4. Palenzona A, Cirafici S. The ytterbium–tin system. J Less Common Met. 1976;46:321–6.
5. Manfrinetti P, Mazzone D, Palenzona A. An up-dating of the Yb–Sn phase diagram. J Alloys Compd. 1999;284:L1–3.
6. Leon-Escamilla EA, Corbett JD. Solid state compounds with tin–tin bonding. $Yb_{36}Sn_{23}$: a novel compound containing oligomeric tin anions. Inorg Chem. 1999;38:738–43.
7. Alejandro A, Leon-Escamilla EA, Corbett JD. Hydrogen impurity effects. A_5Tt_3Z intermetallic compounds between A = Ca, Sr, Ba, Eu, Yb and Tt = Sn, Pb with Cr_5B_3-like structures that are stabilized by hydride or fluoride (Z). Inorg Chem. 2001;40:1226–33.
8. Palenzona A. Dynamic differential calorimetry of intermetallic compounds I. Heat of formation, heat and entropy of fusion of rare earth–tin compounds. Thermochim Acta. 1973;5:473–80.
9. Chatillon-Colinet C, Percheron A, Mathieu J-C, Achard J-C. Calorimetric measurements of the heat of solution of ytterbium in tin. determination of the heat of formation of YbSn3 phase. Compte Rend C. 1970;270:473–6.
10. Witusiewicz VT, Sidorko VR, Bulanova MV. Assessment of thermodynamic functions of formation for rare earth silicides, germanides, stannides and plumbides. J Alloys Compd. 1997;248:233–45.
11. Dinsdale AT. SGTE data for pure elements. Calphad. 1991;15:317–425.
12. Redlich O, Kister A. Algebraic representation of thermodynamic properties and the classification of solutions. Ind Eng Chem. 1948;40:345–8.
13. Sundman B, Jansson B, Andersson JO. The Thermo-Calc databank system. Calphad. 1985;9:153–90.
14. Jansson B. Evaluation of parameters in thermodynamic models using different types of experimental data simultaneously. Thesis, Stockholm: Royal Institute of Technology; 1984.
15. Arroyave R, Liu ZK. Thermodynamic modelling of the Zn–Zr system. Calphad. 2006;30:1–13.
16. Kumar KC, Wollants P. Some guidelines for thermodynamic optimisation of phase diagrams. J Alloys Compd. 2001;320:189–98.
17. Chen SL, Daniel S, Zhang F, Chang YA, Oates WA, Schmid-Fetzer R. On the calculation of multicomponent stable phase diagrams. J Phase Equilib. 2001;22:373–8.
18. Stein F, Palm M, Sauthoff G. Structure and stability of Laves phases part II—structure type variations in binary and ternary system. Intermetallics. 2005;13:1056–74.